Final Report
for
NASA NNG05GI40G

Outer Planets Research Program

Cratering in the Jovian System

Dr. Clark R. Chapman, PI

Dr. William J. Merline, Co-I

Mr. Brian Enke, Research Assistant

Southwest Research Institute, Project 15.11628

for period April 2005 – April 2010

13 July 2010

SwRI, Suite 300, 1050 Walnut St., Boulder CO 80302

Telephone: (303) 546-9670 Email: cchapman@boulder.swri.edu

Programmatic Background

This report summarizes the results of our five-year OPR research program studying cratering of Ganymede and Callisto. The program was initially a three-year effort beginning in April 2005, but was extended via two no-cost extensions due to the press of other obligations. As described in our previous progress reports, work was delayed during 2006 due to an unexpected 10-month-long health disability on the part of Co-I Merline, subsequent urgent requirements of Drs. Chapman and Merline by the MESSENGER project, and other issues.

We have completed the research this spring. This report summarizes the entire research effort, but emphasizes results and interpretations obtained since our previous progress report. We provide extensive illustrations in this report, which will necessarily have to be limited when the research is published in the archival literature.

Project Research Background

The goals of this research project were to study cratering of the Galilean satellites, especially Ganymede and Callisto, in order to learn about implications for the geological evolution of their surfaces and to understand the history of the impacting flux of cosmic projectiles in the Jovian system. Io was not part of our study because it exhibits few if any impact craters. Most of our prior work concentrated on Europa, so this research has concentrated on Ganymede and Callisto. One issue is to gain insight about the role of secondary cratering on these bodies, since secondary cratering has recently been recognized to predominate cratering on Europa (see our paper in *Nature*: Bierhaus et al. 2005), and indeed on Mars and probably elsewhere in the solar system. If secondary cratering dominates small crater populations and has been greatly underestimated or overlooked in the past, then many conclusions emanating from previous studies of the Galilean satellites and other solid-surfaced bodies in the solar system could be wrong. Such conclusions include relative age-dating of different geological units as well as inferences about the size-distributions of small comets and other interplanetary and circumplanetary small-body populations. For this reason, we emphasized studies of smaller craters on Ganymede and Callisto, while not ignoring the larger craters.

Techniques for Measuring Crater Diameters

During the early years of this project, we worked on establishing our methodology for measuring craters (sizes, positions, and morphology class) efficiently, using automated algorithms as an assistant to the analyst who then deletes false or inaccurate crater detections and measurements and adds craters missed by the automated algorithms.

Images were selected to show representative, geologically homogeneous regions taken at good viewing and illumination geometries. Many of the Callisto images were of regions near Asgard, and many of the Ganymede images are of the northern Nicholson region. We show the locations of the image centers in the Appendix on global maps of the two satellites (the rectangles do *not* show boundaries of the areas analyzed. There is a mix of low, medium, and high resolution images. X and Y resolutions were taken from image headers, but X and Y image sizes were calculated manually (in viewer software), varying greatly from image to image. Two images were map-projected via ISIS (c30_5253r and g28_5113r) and ISIS was also used to determine the area of those images. The areas for other images were calculated by multiplying the X and Y resolutions by the X and Y pixel dimensions of the portions selected for measurement .

In order to make the crater detection process more efficient, we used our "automated assistant" approach, developed and refined for application to Ganymede and Callisto in the early phases of the research, as described in earlier annual Progress Reports. We generally used the JPL CSTM crater detection tool (except for g28_2800r). We also used the SwRI-developed Directional Annulus Matlab algorithm to detect craters in one image (c10_2878r).

Outputs from the automated assistant were loaded into the viewing plane of our crater analysis software, described in previous reports, and based on the POINTS software developed at Cornell. The analyst then manually analyzed and refined the automatically detected craters (eliminating non-craters and refining diameters and positions, when necessary, as well as classifying crater morphology as described below). The analyst then searched for craters missed by the automated assistant, and used our software to define the crater rim by 2 to half-a-dozen or more points, which yields the crater diameter, and X,Y coordinates. All automatically generated craters and craters identified by the analyst are assigned a morphology class using our standard 1 to 4 scale (1 = fresh, 4 = highly degraded). Special indicators for "chain" and "elliptical" craters are also assigned.

The crater data are then plotted on R-plots (Crater Analysis Techniques Working Group, 1979), showing log of the spatial density on the vertical axis and log diameter (km) on the horizontal axis. These are essentially differential frequency relations divided by D^{-3}. The data are not plotted vs $\sqrt{2}$ diameter bins, as some researchers do, but rather we select bin widths to best represent the data, using narrower bin widths when statistics are good

and wider ones to avoid bins with zero craters when statistics are poor. We identified a minor issue with some of our narrowest bins (generally at diameters within a few pixels of our resolution cut-off for incompleteness). The automatic tools find craters with quantized diameters (indeed our manual measuring tool is also quantized); if there are a small number of quantized sizes within selected narrow bins, there can be a bit of jumping up and down between neighboring bins that is outside the plotted error bars (which are based on √N counting statistics). The latest version of the CSTM tool searched for craters ranging between 5 and 80 pixels in diameter, using 100 unique crater sizes within the tool (separated with a geometric progression). We believe that quantization is not a major problem.

We plot data for size ranges that have lower limits determined by assessed incompleteness and by the quantization issues described above. Counts are not shown below 6 or 7 pixel diameters. The craters are color-coded on the marked images, and also the data for those craters in the R-plots, using the following scheme: total craters (all classes of craters together) are shown in black (largest symbols on R-plots); classes 1 and 2 combined in blue; class 3 in red; and class 4 in green (the smallest symbols on R-plots). Different images are sometimes plotted on the same R-plot, distinguished by circles, triangles, upside-down triangles, and squares. Sometimes plots on the same graph are of regions associated with each other, but generally not. Eyeball fits to the data are indicated by dotted lines of the appropriate colors.

Results

At the end of this report, in the Appendix, we show – generally on individual pages – illustrations relevant to one or more of the analyzed images. The arrangement is Ganymede first, followed by Callisto. The illustrations generally show an R-plot, the marked images (at the bottom of the page) and, usually, context images, showing the location of the images in an image of a more distant view. There is also brief commentary about the nature of the region. See also the tables and global maps at the beginning of the Appendix. Note that, for simplicity, we refer to the images by the last four digits of the image number (e.g. 5539 stands for c9_5539r).

Callisto. Fig. 1a shows data previously available for Callisto, illustrating the general trend of the crater population ranging from diameters of about 100 m to about 100 km. Fig. 1b shows the total crater counts from the areas researched in this study. Without regard to different terrains, and ignoring morphological classes, these plots show similar trends in the crater size-frequency distribution (SFD) for Callisto. As has long been known (and was not a subject of the present study), there is a decrease in spatial density of craters larger than about 100 km, and there is a peak in the SFD (at about the empirical saturation level) at diameters of a couple tens of km. Towards smaller size craters, there is a dip in the SFD (shallower slope) reaching a minimum at diameters a bit less than 1 km. Toward still smaller diameters, the SFD rises (steeper slope) reaching the empirical

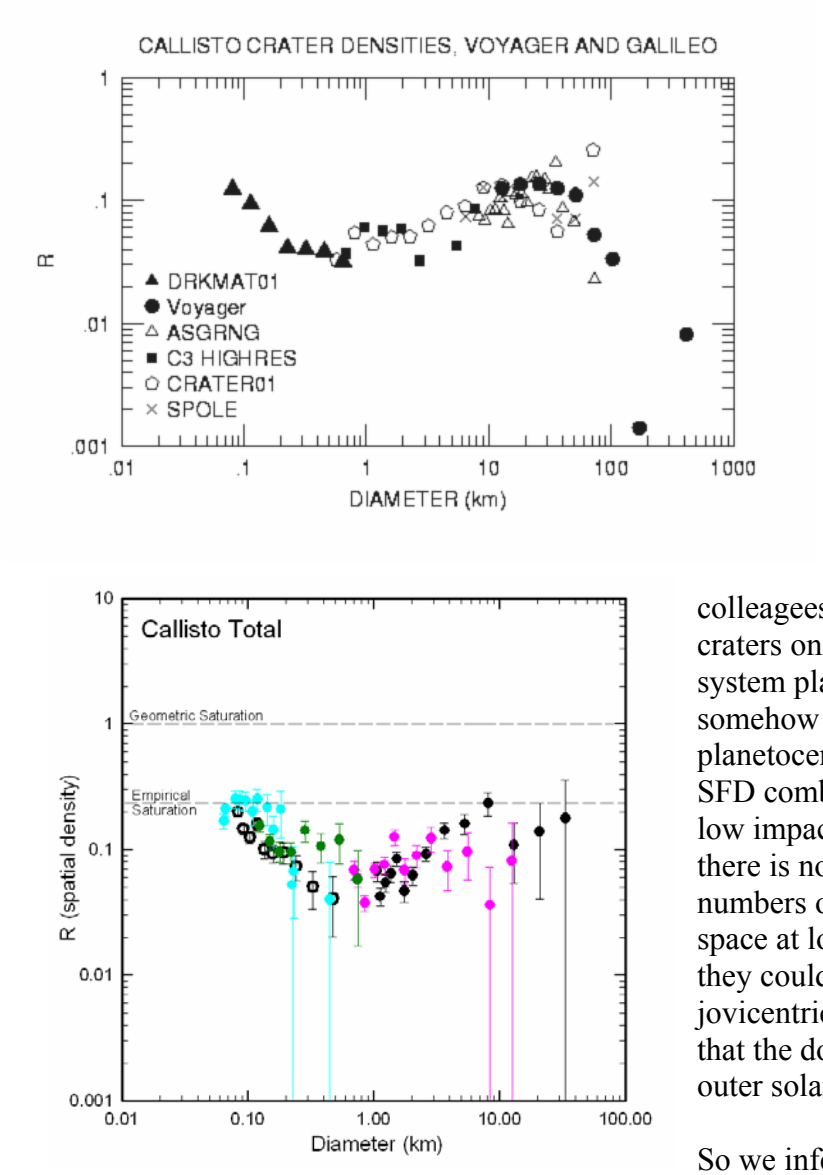

Fig 1 (a, top) Early crater data for Callisto. (b, bottom) Total crater data from the present study.

saturation level at about 100 m, and apparently leveling off at that level for smaller craters.

These attributes of the SFD qualitatively resemble the SFD's for bodies in the inner solar system (e.g. Mercury, the Moon, Mars) if one were to slide the SFD for Callisto a factor of ~5 to the right. This is the basis for the view of Neukum and his colleagees that the source of the craters on moons of outer solar system planets are "asteroids" somehow captured into planetocentric orbits (asteroidal SFD combined with extraordinarily low impact velocities). Of course, there is no known way to get large numbers of asteroids into Jovian space at low enough velocities that they could somehow enter jovicentric orbits. And it *is* known that the dominant impactors in the outer solar system are comets.

So we infer that the SFD for craters larger than ~1 km represent the SFD for the cometary population that dominates cratering in the Jovian system (Zahnle et al. 2003). The branch that turns upward at still smaller diameter we interpret as likely due to secondary craters, especially far-field secondaries, since these are not chain craters. The alternative interpretation, namely that the numerous smaller craters are made by a dominant flux of bodies 10 to 50 m diameter seems difficult to justify, especially since such craters on nearby Europa have been shown to be clustered in a non-obvious but statistically significant way (Bierhaus et al., 2005).

.

In the Appendix, we present images and R-plots for six different regions on Callisto, separately for morphological classes. In general, crater morphologies evolve under continuing erosive and degradational processes in a uniform way such as they retain their nearly-pristine original morphology (classes 1 and 2) for a modest fraction of their lifetimes and much longer durations in the somewhat degraded (class 3) and highly degraded (class 4) states before finally being degraded to the point of non-recognizability. Thus when, at any particular size, the distribution of classes is as just described (and the curves for different classes parallel the curve for total craters), then it suggests a state of equilibrium at all measured scales. This seems to roughly describe the situation for 5539, for instance. Although the overall R-value is decreasing toward smaller diameters, the curves are roughly parallel to within the error bars.

Contrasting with 5539 is 2878, where there is a predominance of fairly fresh craters 5 to 10 km in diameter, but very few fresh craters near and smaller than 1 km. Unlike 5539, this is a region dominated by small, eroding mountains. In the intervening low areas, there are surfaces – perhaps of detritus from the eroding hills – which either do not enable fresh craters to form or else enable them to rapidly erode to more degraded morphology.

For example, 5378 shows a steeply sloping (toward upper-left) SFD for total craters, but classes 1+2 slope the other way, and class 4 is relatively level on the R-plot. So the predominance of craters near 100 m diameter are class 3 craters. Possibly these craters are not formed with pristine morphology (e.g. if they were comparatively low-velocity secondaries from a nearby source). Or maybe the substrate was formed recently and there has not been enough time to completely erase craters, or maybe the substrate has properties that rapidly degrades pristine craters but does not completely erase them.

Image 5453 also shows similar ratios of crater classes in the 100-300 m diameter range. As can be seen in the images of 5378 and 5453 in the Appendix, both regions studied are in the low regions between high, bright mountains. Presumably the sublimation degradation processes and possible landslides of residual lag materials that are common in these regions (Moore et al. 1999) have created similar geology in these two nearby regions. 5453 differs from 5378 in having rather numerous highly degraded craters about 1 km diameter; most of these are located close to the remnant peaks of the large, highly degraded crater that dominates the frame. Perhaps they are marginally preserved from an older epoch of cratering, whereas smaller craters on these slopes are rapidly erased by downlope mass-wasting.

Ganymede. Region 2865 is located east of the palimpsest Buto Facula. Our measurements show a population of very highly degraded craters several tens of km diameter that approaching the empirical saturation density. Otherwise, the more readily visible craters peak, again near the empirical saturation line, around 2 km diameter. Spatial densities near 10 km diameter are similar to that for 2865 (approaching an order of magnitude below saturation) on other medium resolution frames (7800, 2413). Two parts were measured of 2413, both in bright terrain, but one part grooved and the other much less so; the crater SFDs are similar to each other.

Regions 3600 and 3652 are *not* near 2413, even though plotted on the same graph. They are high-resolution images, one in a bright region, the other in a dark region, on opposite sides of a dark/bright boundary. The bright region has a slightly lower crater density (consistent with the stratigraphic relationship that the bright region is younger) but the overall SFDs for the crater classes are similar.

Most of the Ganymede regions we studied show relatively few craters with diameters near 500 to 700 m, but a large number of somewhat smaller craters, reaching empirical saturation densities between 200 and 300 m, and plateauing at that level down to 100 m diameter. (This generality is not true for 3800, which is a region heavily affected by tectonism, which is undoubtedly responsible for the low spatial density of detected craters throughout the size range we sampled [200 m to 3 km diameter].)

The generality *is* true for frames 3539 and 5113. The former is embedded within the latter (see context images in the Appendix), in a bright band. But the rapid variability from near saturation density at 250 m, decrease to minimal R value near 500 m, and return to saturation density (or above) around 700 m to 1 km, we feel is exaggerated by several factors. First, the high-resolution frame 3539 appears to be in a slightly atypical region of the whole 5113 frame, which partly explains its lack of relatively large craters. Second, there may be some residual artifacts enhancing the numbers of relatively small craters on 5113 (the "small craters" being just a bit larger than the "large craters" on the inset frame 3539). An important factor is that the left edge of the portion of the 5113 image we measured is just off the edge of the continuous ejecta blanket of a rather large crater. It is plausible that many of the craters near 1 km diameter are actually near-field secondary craters; indeed, there are several obvious clusters of such craters. The inset frame, 3539, is on the opposite side of 5113, farther from the large crater and away from obvious crater clusters. Nevertheless, examination of 3539 reveals some craters with non-pristine appearance showing some traits resembling near-field secondary craters.

Examining crater classes in the context of our discussion in the Callisto section of the normal parallel curves for cases of steady equilibrium between crater formation and degradation, we can see some deviations in the Ganymede data. For example, there is a relative lack of fresh craters near 1 km diameter in 4000 and, especially, 3800. Since this is the approximate spatial scale of the tectonic grooves and ridges visible in these frames (especially 3800), we suspect that tectonic deformation is particularly efficient at modifying the pristine morphologies of craters of these sizes. Indeed, it is possible that the prominent ridges in the region of 3800 may even prevent fresh craters from forming with a pristine-appearing morphology.

Turning to 4000, it is evident in the context image for the portion of the image that we measured that large-scale deformation processes (probably several) operated here, capable of degrading or even erasing craters many km in diameter. The large, class 3 craters that we measured indicate a scale of degradation that readily explains the lack of fresh craters of these sizes. But there also appear to be processes operating at smaller scales that result in a large fraction of highly degraded small craters a few hundred meters

in size. It is probably not possible to rely on crater SFDs to unravel the complex geological history of this region.

Cratering of the Icy Satellites. As has been known since the Voyager flybys of the Galilean satellites, Callisto is a relatively simple world. It is heavily cratered and generally lacks the complex subsequent tectonism, formation of bright grooved bands, and other features of Ganymede. Of course, as shown in Fig. 1a but not explored in the present study, the largest craters on Callisto (>100 km diameter) are deficient, and what mainly remain are palimpsests. Smaller craters are subject to degradation by the sublimation degradation process and related mass wasting, but the basic production function remains generally visible. The detritus that fills the lower areas of Callisto provide relatively smooth plains for recording the smallest craters, several hundred meters in size and smaller. In general, the shapes of crater SFDs for Callisto (Figs. 1a and 1b) resemble that for Europa (Bierhaus et al. 2009), except at higher spatial densities, because Callisto's surfaces are not so youthful.

While the largest craters on Callisto are quite old, the smaller craters are clearly younger, reflecting the ongoing degradation process, so Figs. 1a and 1b do not represent a production function throughout the size range. Note that the steep branch for small craters on Callisto commences at a smaller size (~300 m) than for Europa (~1 km), presumably reflecting the loss of all but the most recent small craters due to the ongoing sublimation degradation processes on Callisto. Indeed, assuming we are correct that the process is ongoing, it probably affects smaller craters more efficiently than larger ones, so the steep branch of the production function is probably considerably steeper, in actuality, than indicated by our crater measurements. That would make the steep branch quite similar to what is observed on Europa, and that has been demonstrated to be due to secondary craters rather than primary cratering.

Ganymede obviously must be cratered by the same population of impactors as the nearby moons Callisto and Europa, yet many of the SFDs we have measured look different. Ganymede also shows a deficiency of craters >100 km diameter, but that was not the focus of our study. Our studies of Ganymede do not generally show the gradual decline in crater densities from ~30 km to ~500 m seen on Callisto. Region 2865 shows a relative enhancement near 2 km and other regions show peaks at diameters <1 km. Because of the wide differences from region to region, and even apparently within regions (cf. 5113 and 3539), it appears that the spatially varying, comparatively recent geological activity on Ganymede (tectonism, etc.) has partially erased clear records of the primary and secondary cratering production functions.

As we have shown, there is a correspondence between the varying cratering SFDs on Ganymede and the first-order geological processes that have operated in the corresponding regions; more detailed crater studies might elucidate the history of these processes. But Ganymede is difficult to study. Given the relatively limited lighting and viewing geometries of the Galileo imaging, and the diverse small-scale albedo patterns common on Ganymede, it is more difficult to recognize and classify craters on Ganymede than for other bodies, even geologically complex bodies like Mars. On the basis of the

research we have done on Ganymede, however, we find nothing that detracts from our conclusion that the same kind of cratering has occurred on Ganymede as has occurred on Europa and Callisto; we find the latter to be compatible, excepting chiefly the substantial age differences between Europa and Callisto.

References

E. B. Bierhaus, C.R. Chapman, W.J. Merline, 2005. Secondary craters on Europa and implications for cratered surfaces, *Nature* 437, 1125-1127.

E.B. Bierhaus, K. Zahnle, C.R. Chapman 2009. Europa's crater distributions and surface ages, in "Europa" (ed. R.T. Pappalardo et al., Univ. Ariz. Press, Tucson), 161-180.

Crater Analysis Techniques Working Group 1979. Standard techniques for presentation and analysis of crater size-frequency data, *Icarus* 37, 467-474.

J.M. Moore & 13 co-authors 1999. Mass movement and landform degradation on the icy Galilean satellites: Results of the Galileo nominal mission, *Icarus* **140**, 294-312.

K. Zahnle, P. Schenk, H. Levison, L. Dones 2003. Cratering rates in the outer solar system, *Icarus***163**, 263-289.

Appendix

Ganymede Images Measured

IMAGE_NUMBER	LATITUDE	LONGITUDE	RESOLUTION_m	AREA_sq_km	REGION
g8_2865r	11.830	189.994	153x154	14891.77	Sanshar
g28_3800r	-15.475	346.391	46.4x35.0	974.77	Arbela
g28_5113r	-15.798	311.741	114.42x114.42	3539.98	Smooth02
g28_3652r	-14.267	320.045	22.0x21.9	36.3157	dark
g28_3600r	-14.444	318.844	20.6x19.8	55.8592	bright
g28_3539r	-15.900	310.677	16.4x16.7	24.6492	Smooth01
g8_7800r_sub1	40.458	192.804	968x1279	34820.8	"light" section of regional co ntext image
g8_7800r_sub2	40.458	192.804	968x1279	33706.5	"dark" section of regional con text image
g8_2413r_sub1	-29.261	178.741	195x231	5581.08	Caldera-like features
g8_2413r_sub2	-29.261	178.741	195x231	5070.94	Caldera-like features
g28_4000r	-24.498	316.852	43.5x46.4	317.898	Caldra01

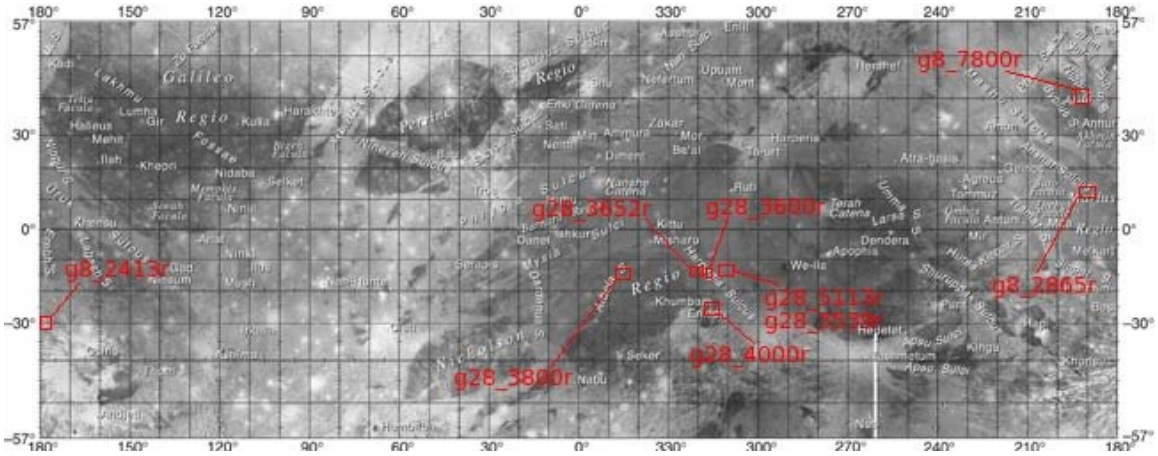

Callisto Images Measured

IMAGE_NUMBER	LATITUDE	LONGITUDE	RESOLUTION_m	AREA_sq_km	REGION
c30_5253r_sub1	12.303	120.758	8.6x8.6	4.44	Asgard HiRes_01
c30_5253r_sub2	12.303	120.758	8.6x8.6	5.6949	Asgard HiRes_01
c9_5539r	-7.428	5.371	175x159	12608.9	crater01
c10_2878r	20.514	142.251	94x99	4549.94	Asgard
c30_5378r	14.266	139.892	12.4x10.7	53.32*	Asgard HiRes_02
c30_5453r	12.377	140.474	16.7x14.6	50*	Asgard HiRes_03

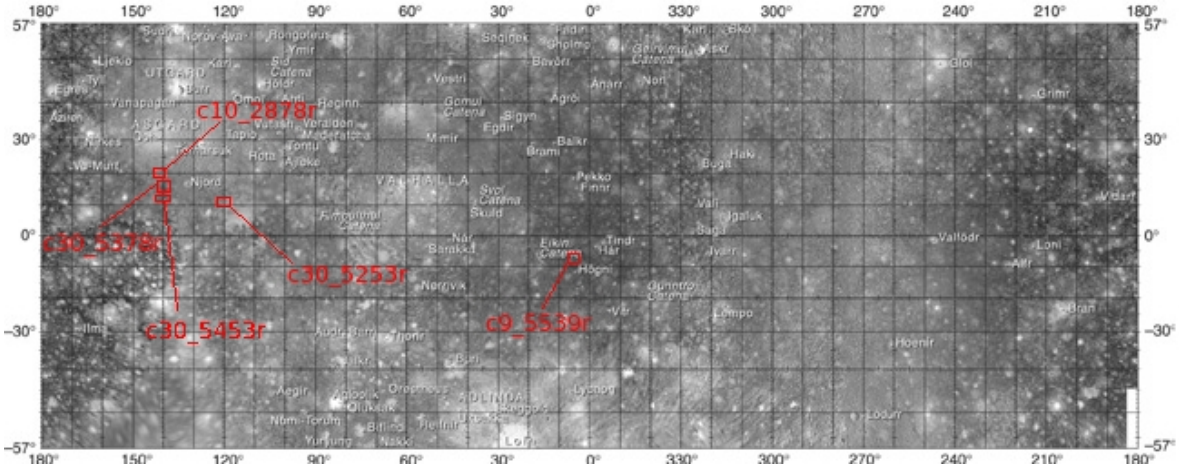

Center locations of frames are shown on context maps, but rectangles do not indicate frame boundaries.

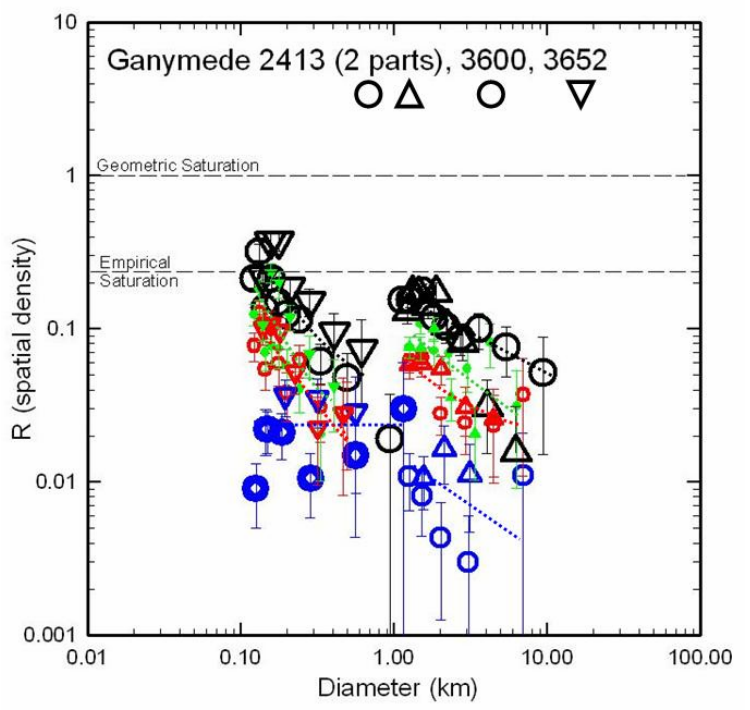

Context images: 3600

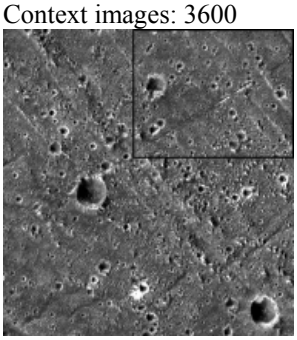

3652

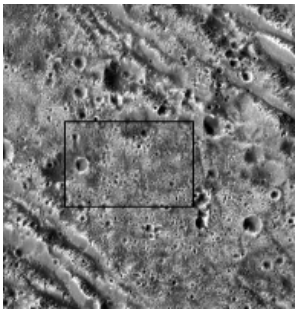

3600 is in bright region near dark/bright boundary; 3652 in adjacent dark flat region.

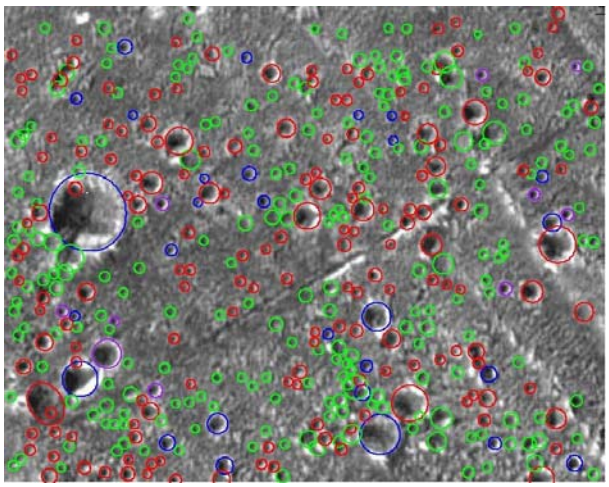

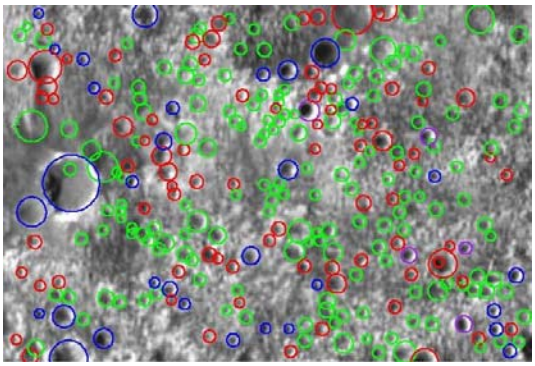

3600 left, 3652 above
2413 sub 2 below; more graben and chains.

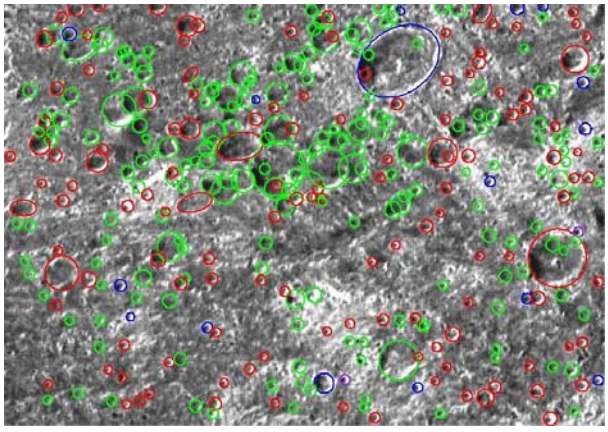

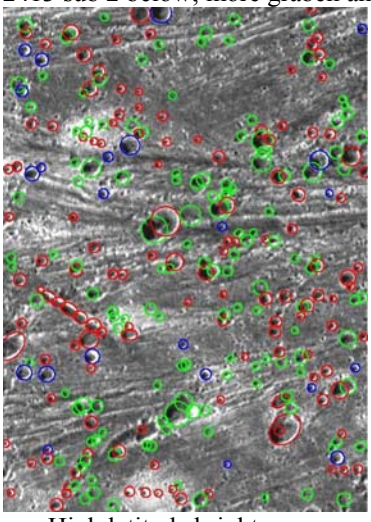

2413 sub. 1. Flat area with fewer graben, some chain craters. High latitude bright area near rays.

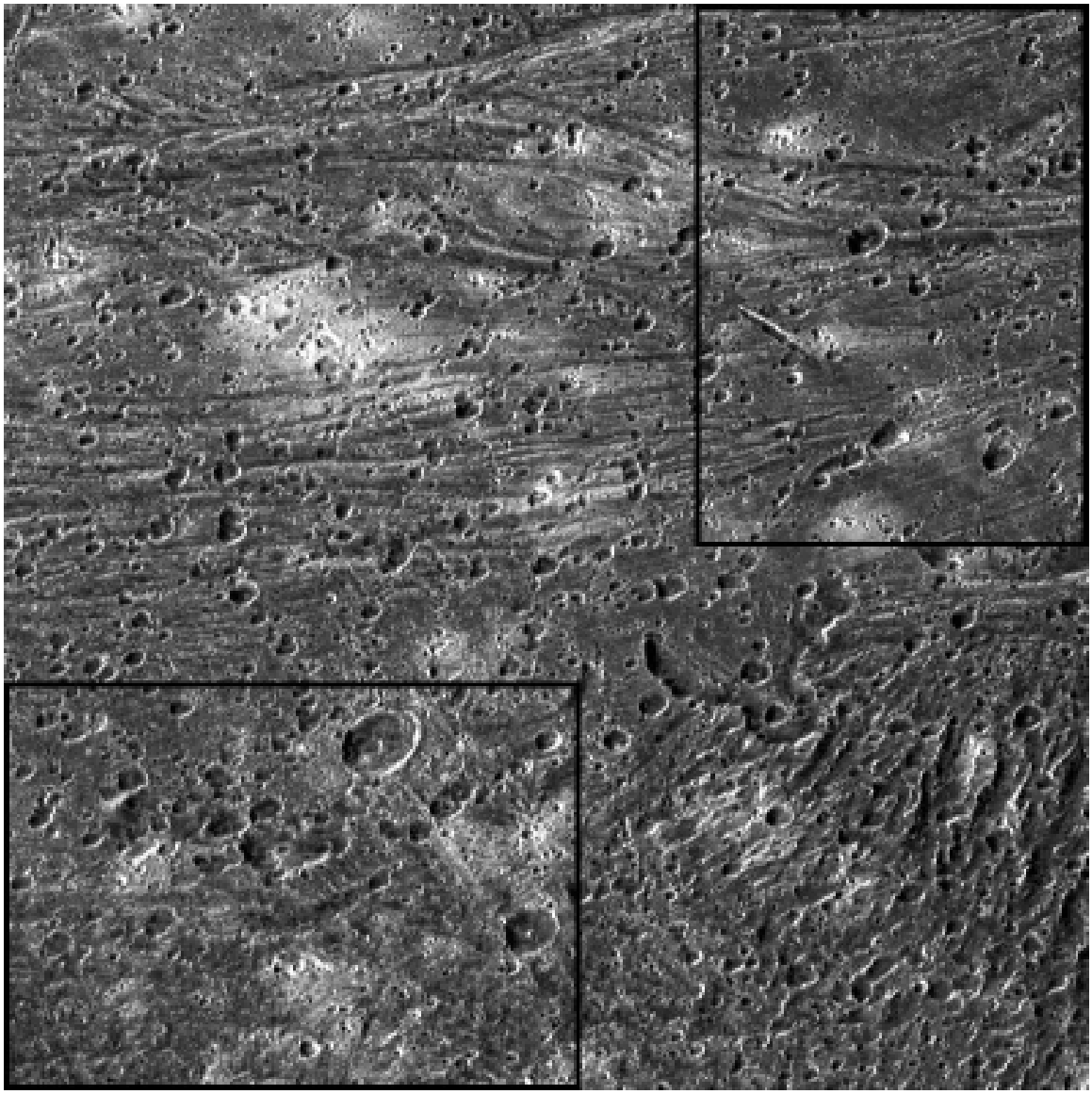

Context image for two parts of 2413.

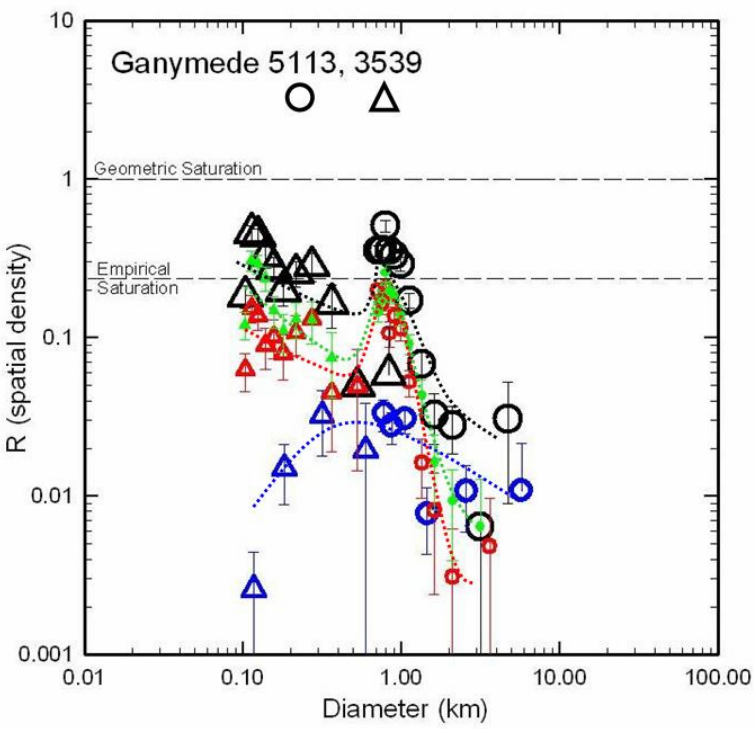

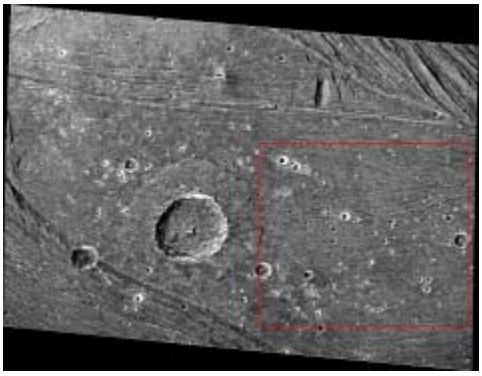

Context image for 5113.

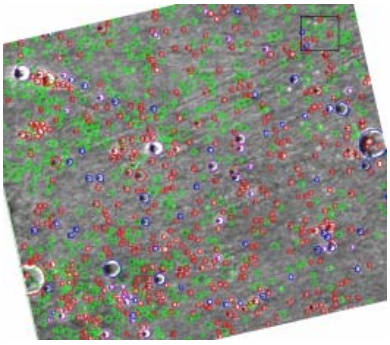

Relationship of nested images: black rectangles show location of 3539 (lower left measured image) within 5113 (lower right).

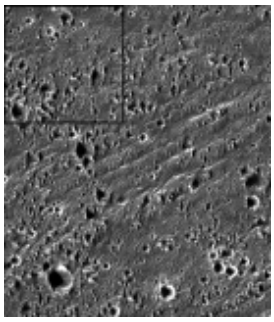

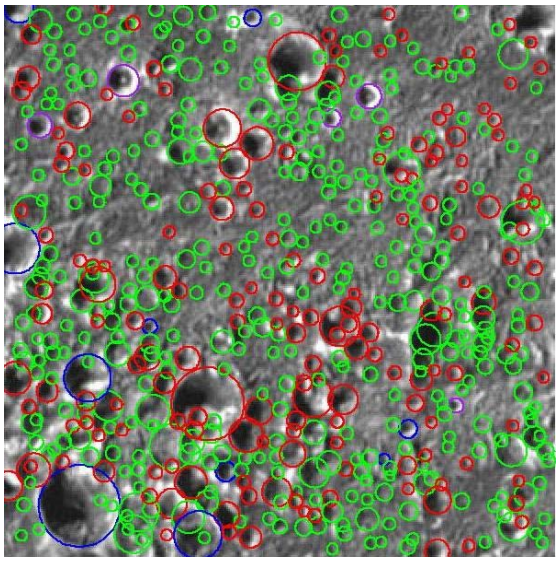

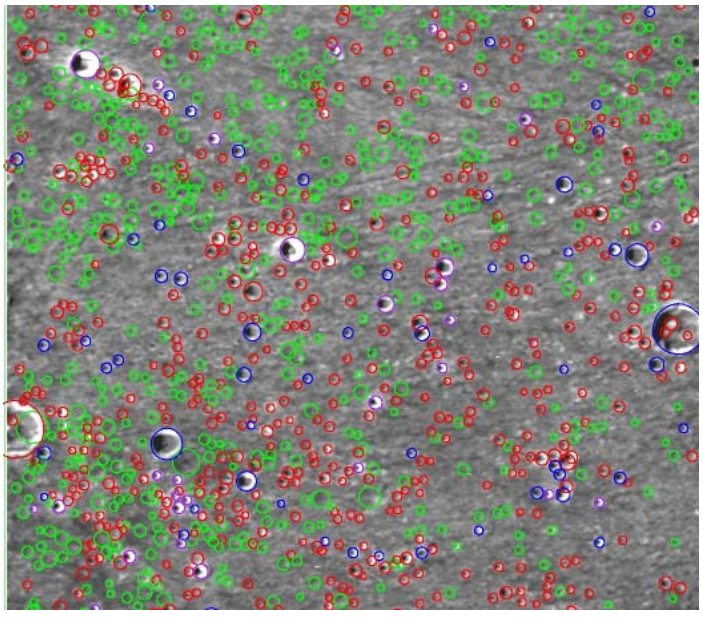

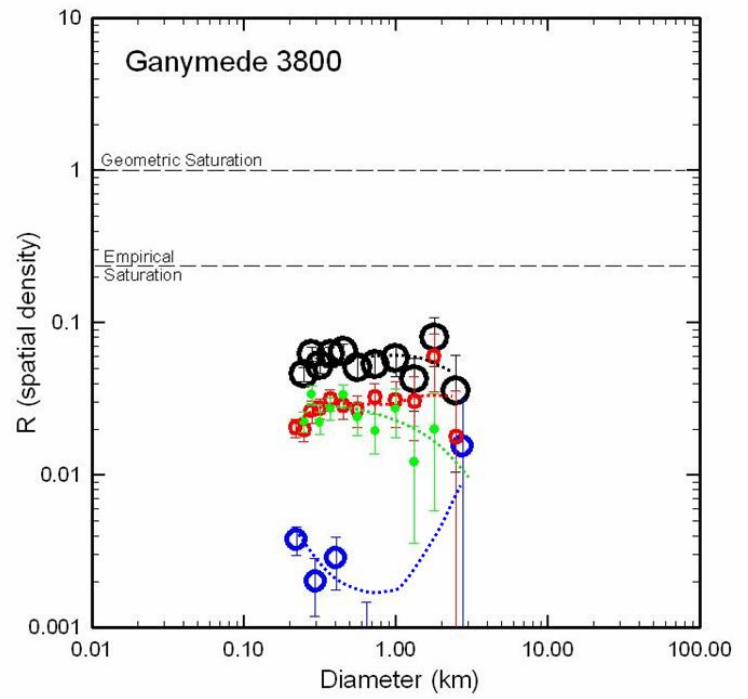

Dark furrowed region adjacent to bright, furrowed band.

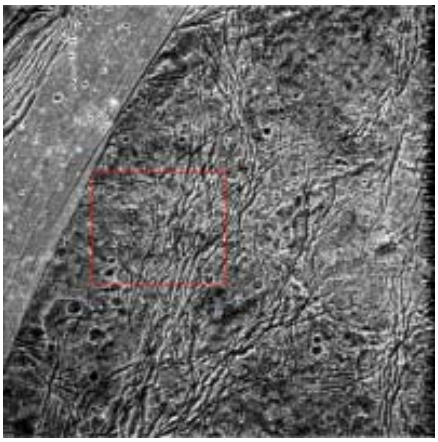

Context image.

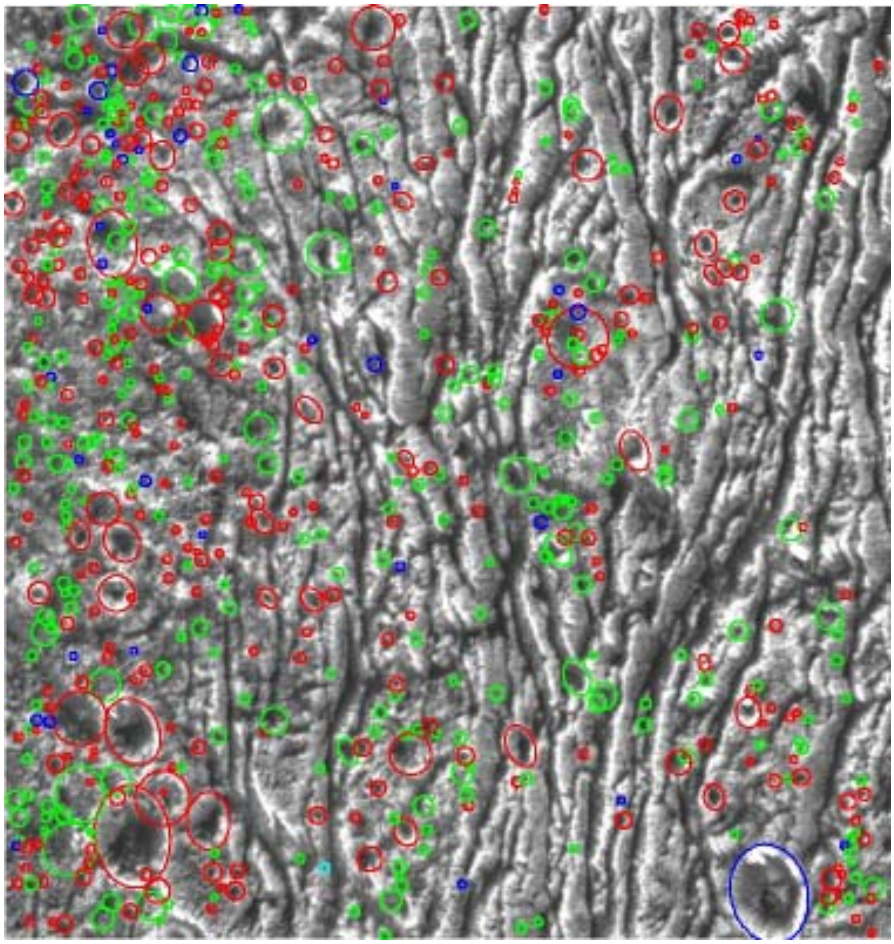

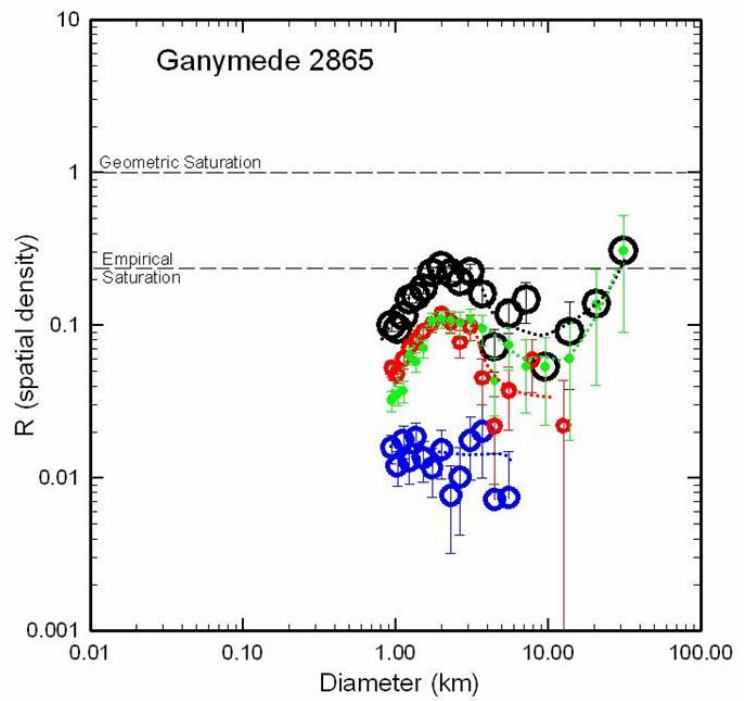

Cratered, dark region.

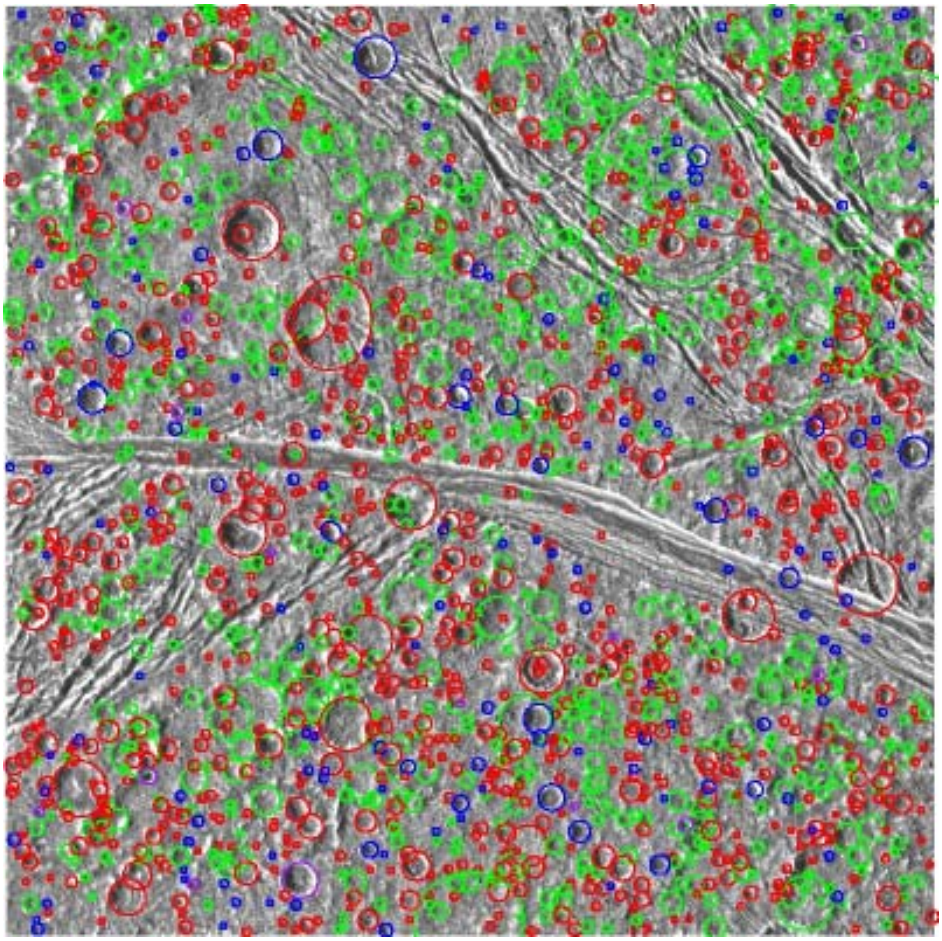

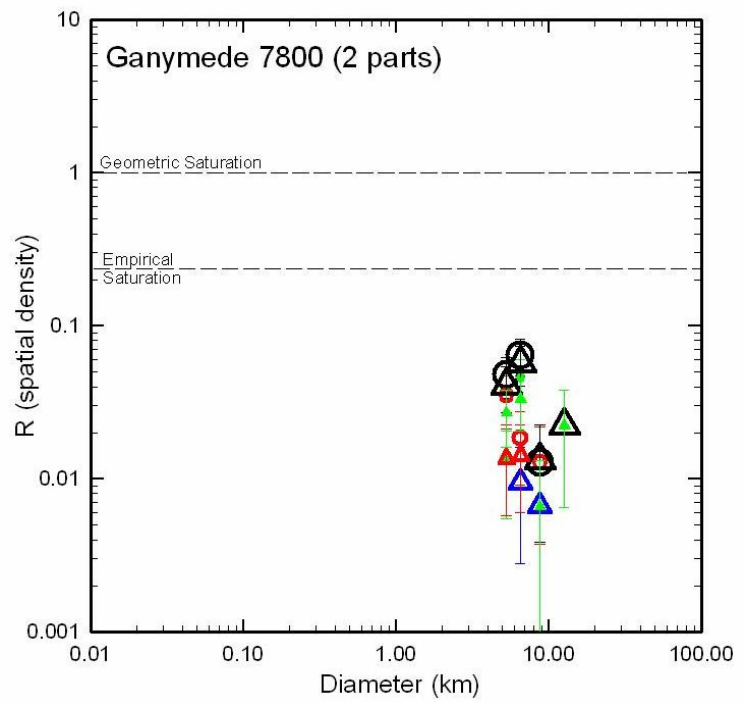

Subregion 1 (circles) is small bright region; subregion 2 (triangles) is small mottled dark region.

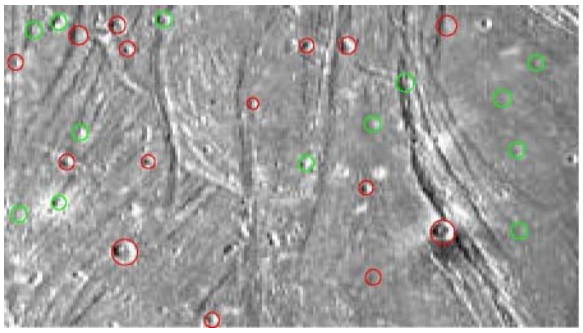

Two modest parts of 7800 and context image.

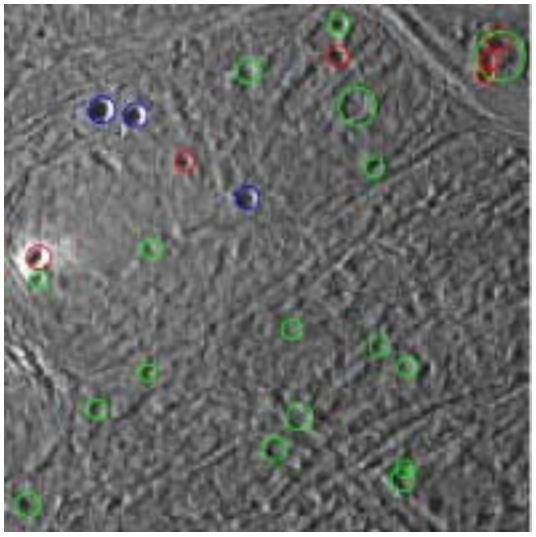

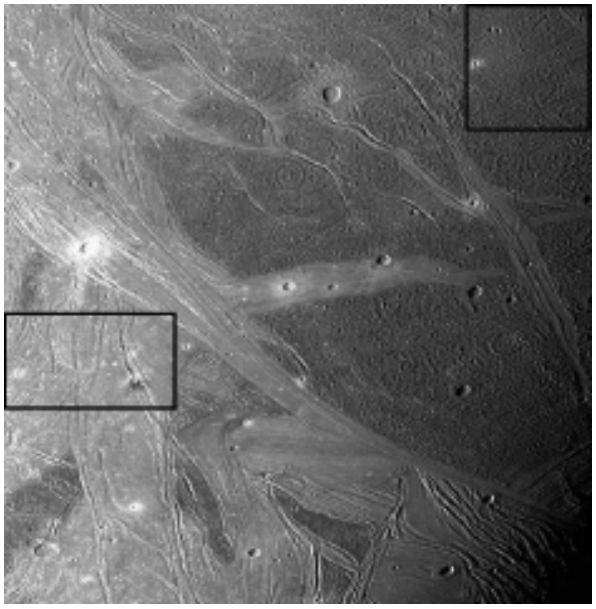

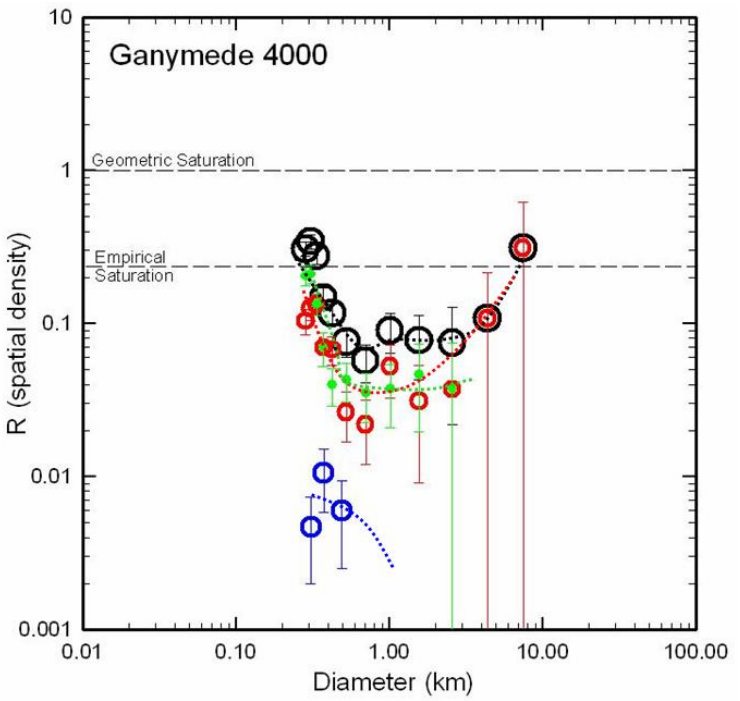

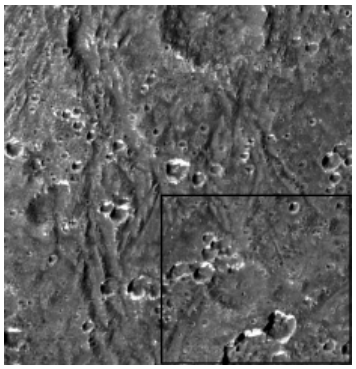

Context image.

Cratered, mottled, furrows.
Intermediate albedo.

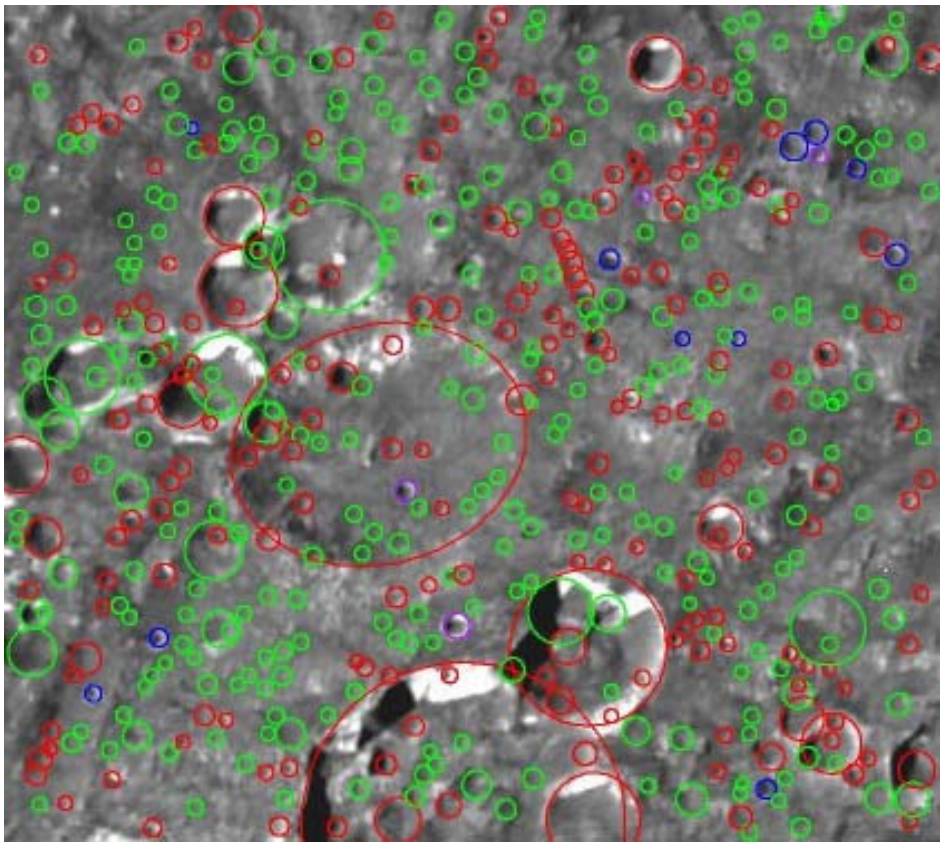

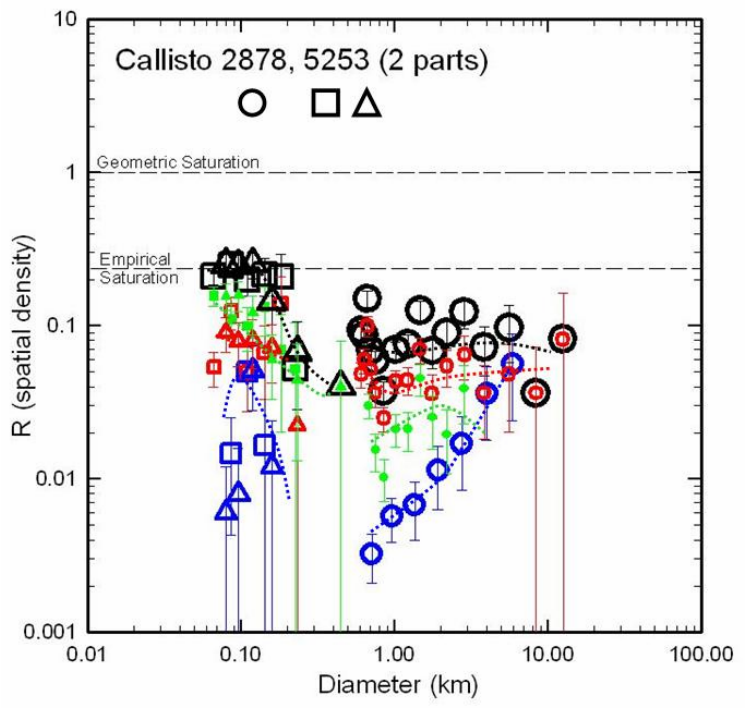

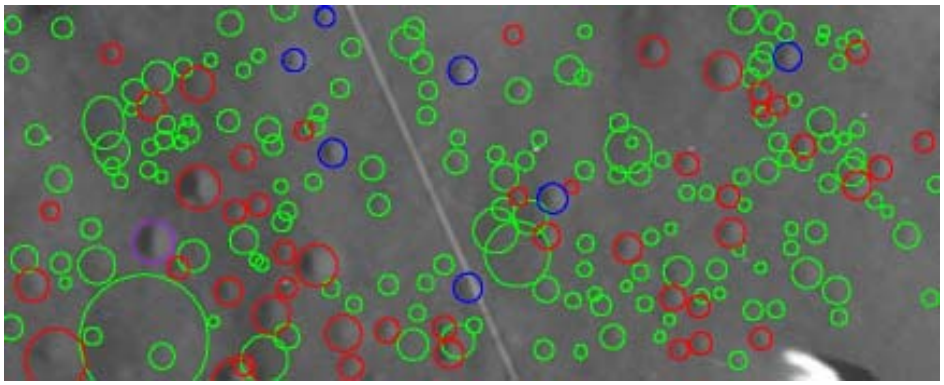

5253 sub 1 (squares) below, 5253 sub 2 (triangles) above; 2878 (circles) lower right.

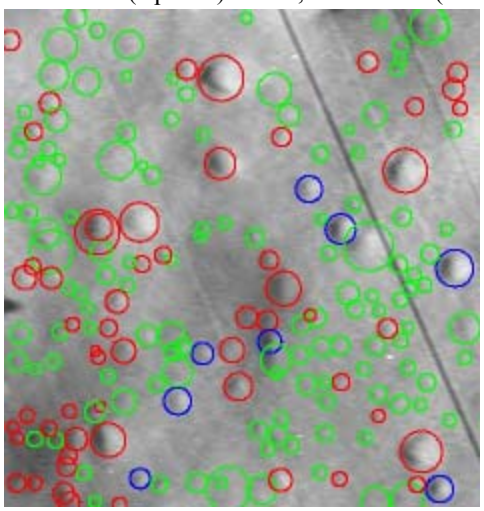

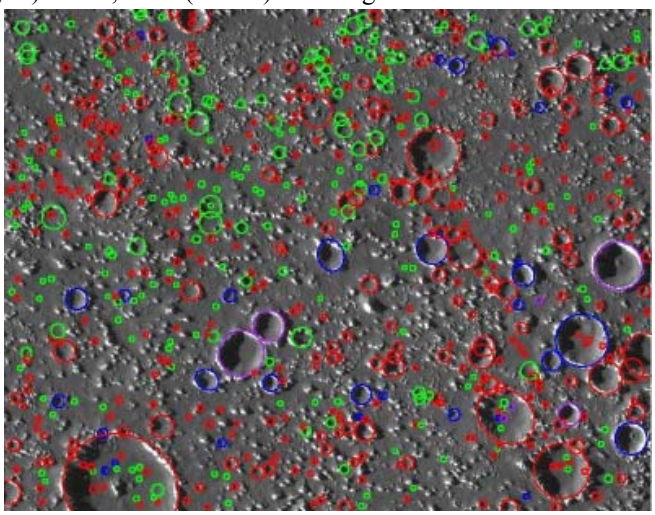

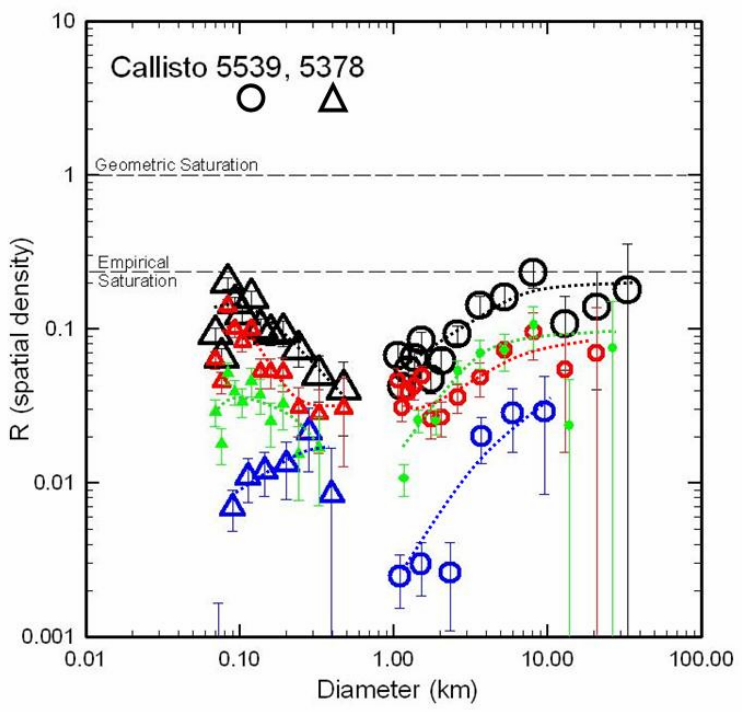
Callisto 5539, 5378
Geometric Saturation
Empirical Saturation
R (spatial density)
Diameter (km)
10
1
0.1
0.01
0.001
0.01
0.10
1.00
10.00
100.00

5539

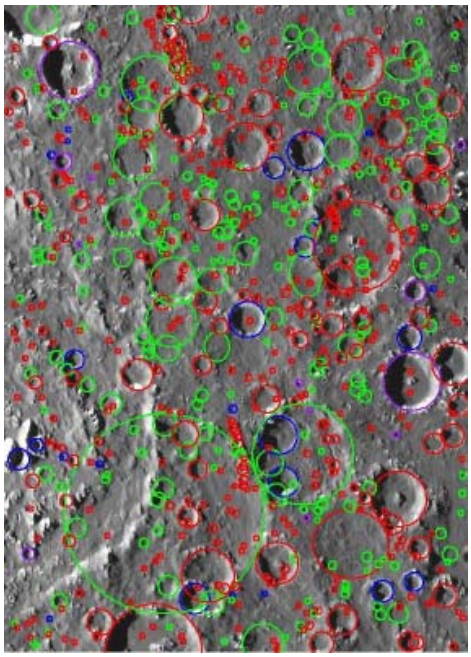

5378

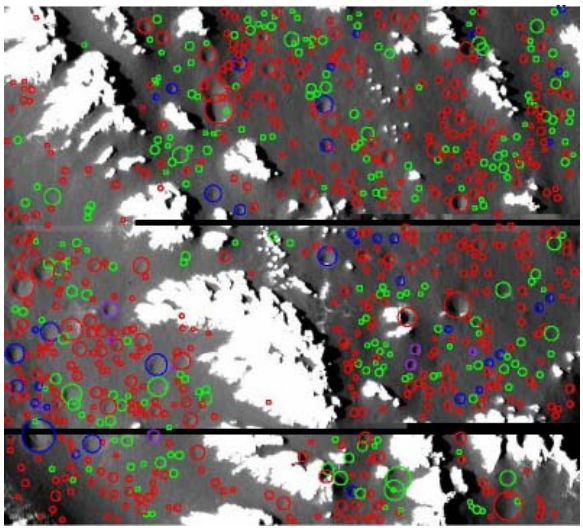

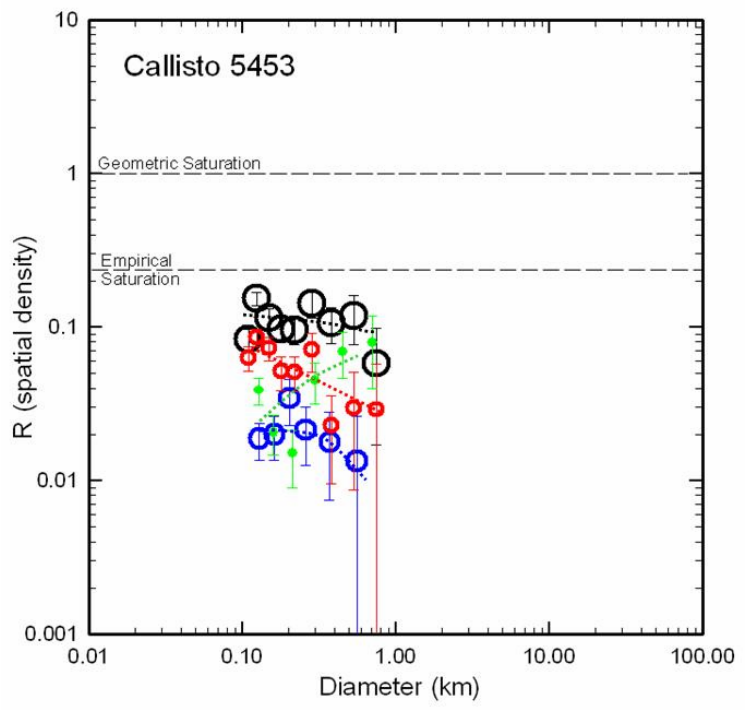
Callisto 5453
Geometric Saturation
Empirical
Saturation
R (spatial density)
Diameter (km)
10
1
0.1
0.01
0.001
0.01
0.10
1.00
10.00
100.00